Effect of Doped CeO with Si3N4 Powders on the Densification Mechanism During

Yao Liu (liuyao1985@csu.edu.cn)
Pingxiang University

Research Article

Keywords: SPS, Si3N4 ceramics, Doped, Liquid phase sintering

Posted Date: January 4th, 2021

DOI: https://doi.org/10.21203/rs.3.rs-136510/v1

Yao Liu[a,*], Zijian Hu[a], Zhuo Li[a],Lina Zhan[a,*],Lin Cheng[a,*],Lijin Cheng[b,*]

[a]College of Mechanical and Electronic Engineering, Pingxiang University, Pingxiang, 337000, China

[b]School of Mechanical Engineering, Heibei University of Technology, Tianjin, 300130, China

ABSTRACT

The densification mechanism of doped CeO with Si_3N_4 powder during Spark Plasma Sintering (SPS) was investigated under temperatures ranging from 1500 to 1750 °C at soaking pressures of 30, 40, 50 MPa. Results showed that the relative density of Si_3N_4 ceramics sintered at 1650 °C and 30 MPa was 97.9%. A creep model was employed to determine the mechanism, which can be interpreted on the basis of the stress exponent (n). The results showed that the mechanism was controlled by liquid phase sintering at low effective stress regime (n=1).

Keywords: SPS; Si_3N_4 ceramics;Doped;Liquid phase sintering

1 Introduction

Owing to their low thermal expansion,high wear resistance,good thermal shock resistance, Si_3N_4 ceramics are suitable for many applications such as aerospace and military [1-3]. Although Si_3N_4 ceramics have been used in various fields, poor sintering performance due to the strong covalent bond of Si-N hinder the futher application of Si_3N_4 ceramics[4-5]. Traditionally, Si_3N_4 powders have reached only 90 % relative density via press-less sintering. SPS is an advanced sintering method that has great potential for application in density

---

* Correspondingauthor. Tel.: +86799 6682029; Fax.: +86 799 6682029

E-mail address:liuyao1985@csu.edu.cn,24599437@qq.com(Lina Zhan),rymw27@163.com (L. Cheng)and ljcheng@hust.edu.cn (L. Cheng).

ceramics [6-9]. Compared with other sintering techniques, this technology shortens soak time and lowers sintering temperature. Therefore, SPS is suitable for the investigation of the densification mechanism of Si_3N_4 powder.

The model [10-12] has been widely used to describe the SPS densification mechanism of ceramic materials. Cheng *et al.* [13] studied consolidated 0.7 $CaTiO_3$-0.3 $NdAlO_3$ ceramics through SPS and indicated that densification during SPS is controlled by dislocation motion. Zhang *et al.* [14] found that the densification of B_4C powder was controlled by grain boundary slip.Deng *et al.* [15] examined tungsten powder during the SPS process and found that densification was governed by grain boundary diffusion and creep deformation. Therefore, analysis of the densification mechanism using the creep model during the SPS process is feasible. However, there were few attention to the utilization of rare-earth oxides as sintering additives, especially SPS. Greskovich *et al.* [16] and Hoffmann *et al.* [17] studied rare-earth oxides as sintering additives and found that their phase composition could be controlled during SPS. German [18] and Kitayama [19] pointed out that the densification mechanism of rare-earth element doping was controlled by grain boundary diffusion under TEM observation. There have been some studies on the densification process of rare-earth element doping; however, the densification mechanism remains unclear compared with that of Si_3N_4 powders at a high temperature during SPS.

In this study, the Si_3N_4 powders were consolidated through SPS at temperatures ranging from 1500–1750 °C, fixed pressure levels ranging from 30–50 MPa, and a soaking time of 30 min for studying the densification mechanism as a function of SPS were described using the creep model and verified using microstructural observation.

2 Experimental Section

Si_3N_4 powder (800 nm, purity > 99.5%, Aladdin, China) was used as a new material. CeO powders (800 nm, purity > 99.5%, Aladdin) were used as sintering additives. A certain

amount of Si_3N_4 and CeO powders were mixed in the ball mill for 12 h.The powder was then dried in a drying oven after ball grinding. Then placed in Muffle furnace for 2-4 hours during 600-800 °C.Finally, the mixed powder was obtained by passing through 80 meshes.

All tests were conducted with the mixed Si_3N_4 powder in vacuum (GmbHGewerbepark 16 96528 Rauenstein, Germany). The pressure of 30-50 MPa was selected for the sintering temperature ranging from 1500–1750 °C for 30 min. The relative instantaneous density of the sample in each period of sintering was calculated using the following equation:

$$D = \left(\frac{L_f}{L} \right) D_f \quad (1)$$

Where D is the instantaneous relative density, L_f is the final height, L is the instantaneous height, and D_f is the final relative density.

Vickers hardness test was carried out on the digital Vickers hardness tester (HVS-50, Hefei Kejing Company). The test samples were polished to mirror surface on sandpaper of 80 mesh, 400 mesh, 1000 mesh and 2000 mesh respectively. The test load was 20 kg and the loading time was 10 s. The calculation formula is as follows:

$$HV_{SN} = 0.1891 \frac{F}{d^2} \quad (2)$$

Where, HV_{SN} is the Vickers hardness (GPa) of Si_3N_4 sample; F is loading pressure of pressure head (N); d is diagonal of indentation(m).

The fracture toughness of Si_3N_4 was measured by Vickers indentation method. The sample with indentation was sprayed with gold to obtain the crack length. The crack load was 20 Kg, and the pressure of the head was 196.2 N. The calculation formula is as follows:

$$K_{IC} = 0.0899 (HV_{SN} \times P / 4l)^{\frac{1}{2}} \quad (3)$$

Where, HV_{SN} is the vickers hardness (GPa) of Si_3N_4 sample; P is loading pressure of

pressure head (N); l is crack length (m).

The crystal structure was observed via an X-ray diffractometer (Ultima IV, Rigaku, Japan). The morphology of ceramics was observed using a field emission scanning electron microscope (Quanta 250 FEG, FEI, USA). The possible mechanisms was studyed via Transmission electron microscopy(TEM, JEM-2100F,Japan).The samples for TEM were grounded by sandpaper and thinned down to perforation by twin-Jet Electropolisher(MTP-1A,SHANGHAI JIAODA Inc., China).

3 Results and discussion

Figure 1 shows the curves of relative density and densification rate. The densification rate evidently exhibits a clear peak centered at approximately 1650 °C. The densification of Si_3N_4 ceramics evidently begins at 1400 °C and stops at 1800 °C. However, there is no densification below 1400 °C. Therefore, the sintering temperature was finally set to approximately 1650 °C (1550–1700 °C) and the sintering pressure was controlled at 30–50 MPa to obtain an optimal densification rate.

The densification curves of as-sintered Si_3N_4 ceramics at 1550–1700 °C are shown in Fig. 2a, which shows that the densification curve change trend of Si_3N_4 ceramics was similar under the following conditions: temperature and pressure ranges of 1550–1700 °C and 30–50 MPa. The sintering temperature increased from 1550 to 1700 °C, and the relative density of Si_3N_4 ceramics increased significantly from 86.6% to 98.8%. Figure 2b shows that when the sintering temperature is relatively higher (1600 °C), increasing the pressure significantly improves the relative density of the sample and enhances the densification effect. When the sintering temperature of SPS was 1600 °C, the pressure increased from 30 to 50 MPa, and the relative density of samples increased from 89.2% to 97.8%.

Fig.3 shows the XRD patterns of Si_3N_4 ceramics prepared by sintering. As shown, the crystal phase of as-sintered Si_3N_4 ceramics is β-Si_3N_4 and $Ce_{4.67}(SiO_4)_3O$ of the crystalline

phase at the grain boundary[4]. This is because Ce^{3}+ reacts with Si_3N_4 and the oxide SiO_2 on the particle surface to produce the Ce-Si-O-N eutectic phase. Combined with the ternary phase diagram of the Si_3N_4-Ce_2O_3-SiO_2 system, CeO_2 reacts with Si_3N_4 at 1500 °C to form amorphous phase $Ce_{4.67}(SiO_4)_3O$ and crystallizes during the cooling process, providing a fast channel for the densification of Si_3N_4 ceramics. It is observed clearly in Fig. 7(a) that amorphous phase $Ce_{4.67}(SiO_4)_3O$.

Figure 4 shows the SEM image of the Si_3N_4 ceramics at different temperatures and pressures. Figure 5 shows the grain average size of the Si_3N_4 ceramics. Figures 4 and 5 together show that when the pressure is constant, grain size and sample density increase as the sintering temperature increases. Table 1 showes the mechanical properties of Si_3N_4 ceramics sintered by SPS at different temperatures and pressures. It is observed clearly that the bending strength of sample with the increase of sintering temperature and pressure, the bending strength of sample and vickers hardness, fracture toughness is reduced, because with the increase of temperature and pressure, the increase in the number of β-Si_3N_4 phase, promoted the flexural strength and the vickers hardness of sample, weakened the specimen fracture toughness.

To better explain the above phenomena, the steady state creep model was used to further account for the densification mechanism [20-22]:

$$\frac{1}{\mathrm{D}}\frac{dD}{dt} = A\frac{\phi\mu_{eff}b}{kT}\left(\frac{b}{G}\right)^{p}\left(\frac{\sigma_{eff}}{\mu_{eff}}\right)^{n} \qquad (4)$$

where D is the instantaneous relative densification; A is the diffusion coefficient, which is constant; b is the Burgers vector; k is the Boltzmann constant; T is the temperature; G is the grain size; P is the grain exponent; n is the stress exponent; μ_{eff} is the instantaneous shear modulus; and σ_{eff} is the instantaneous effective stress; μ_{eff} and σ_{eff} can be further expressed by the following equation:

$$\sigma_{eff} = \frac{1-D_0}{D^2(D-D_0)}\sigma^{mac} \quad (5)$$

$$\mu_{eff} = \frac{E_{th}}{2(1+v_{eff})}\frac{D-D_0}{1-D_0} \quad (6)$$

where D_o is the densification; $\sigma^{\max}$ is the mac compaction stress; E_{th} is Young's modulus; and V_{eff} is the effective Poisson's ratio. The thermodynamic diffusion coefficient is expressed as follows:

$$\phi = \phi_0 \exp(-Q/RT) \quad (7)$$

where ϕ_o is the diffusion factor; Q is the activation energy; and R is the gas constant. Combined with Equations 6, 7, 8 and 9, the model can further be expressed as follows:

$$\frac{1}{\mu_{eff}}\frac{1}{D}\frac{dD}{dt} = K\frac{e^{\frac{-Qd}{RT}}}{T}(\frac{b}{G})^p\left(\frac{\sigma_{eff}}{\mu_{eff}}\right)^n \quad (8)$$

where K is a constant, and Q_d is the relative activation energy. Considering that the grain size changes little during this experiment, b/G can be assumed to be a constant, and Formula 10 can be further expressed as:

$$\frac{1}{\mu_{eff}}\frac{1}{D}\frac{dD}{dt} = K\frac{e^{\frac{-Qd}{RT}}}{T}\left(\frac{\sigma_{eff}}{\mu_{eff}}\right)^n \quad (9)$$

To determine the value of n, the relative activation energy is assumed to be a constant at a certain temperature. The logarithm of both sides of Formula 11 is obtained, and then, Formula 11 can be rewritten as:

$$in(\frac{1}{\mu_{eff}}\frac{1}{D}\frac{dD}{dt}) = nin\left(\frac{\sigma_{eff}}{\mu_{eff}}\right) + K_1 \quad (10)$$

where K_1 is a constant, and the required value of n can be obtained by calculating the slope value.

Figure 6 shows the effective stress exponent at different sintering temperatures. Through the calculation of the above model, it can be concluded from the figure that at 1500–1600 °C, the values of n are relatively small (approximately equal to 1).Under low effective stress (n = 1), the densification mechanism of Si_3N_4 ceramics is mainly controlled by liquid

phase sintering due to the occurrence of amorphous phase at low melting point.

In previous studies [23-27], the model has been studyed in the analysis of the densification mechanism in the SPS process . Guillanume [28] *et al.* sintered zirconia with SPS and proposed the hypothesis stating that when the stress exponent is 2, the densification mechanism of SPS is mainly controlled by grain boundary slip. Santanach *et al.* [29] studied the discharge plasma sintering of Al_2O_3 and concluded that when the stress exponent is 2.1, the densification mechanism is mainly controlled by grain boundary slip regulated by lattice diffusion. Gendre *et al.* [30] found the densification mechanism of zirconium carbide powder SPS and calculated that when the stress exponent is n≈1, the densification is dominated by liquid phase sintering. Therefore, in the current study of SPS density Si_3N_4, the densification mechanism of Si_3N_4 ceramics is mainly controlled by liquid phase sintering within the temperature range of 1500–1600 °C.

To further confirm the densification mechanism caused by liquid phase sintering, the sintered samples with a sintering temperature of 1600 °C, pressure of 50 MPa, and holding time of 30 min were selected for TEM characterization. In Fig. 7a, dislocation and twins are not observed. Mapping analysis at the grain boundary shows the presence of Si, N, and Ce elements at the grain boundary, as illustrated in Fig. 7b. Within the aforementioned temperature range, the effective stress state is relatively lower, and the densification mechanism of SPS sintered Si_3N_4 is mainly controlled by liquid phase sintering.

4 Conclusions

In this study, the densification mechanism of Si_3N_4 powder in SPS, with temperature in the range of 1500–1700 °C and pressure in the range of 30–50 MPa for 30 min heat preservation, was studied using a high temperature creep equation. During the densification process, indicating that the densification mechanism was caused by the liquid phase sintering.

Acknowledgement

This work is funded by the National Natural Science Foundation of China (51805187), Shenzhen Science and Technology Innovation Commission Technology Research Project (Grant Nos 20170410221235842), Key R&D Project of Jiangxi Provincial Department of Science and Technology(20203BBE53053).The State Key Laboratory for Powder Metallurgy at Central South University is acknowledged.

References

[1] N. Kondo, Y.Suzuli, T. Ohji. Superplastic sinter forging of Silicon Nitride with Anisotropic Microstructure Formation, J. Am. Ceram. Soc. 82 (1999) 1067-1069.

[2] D. Suttor, G. S. Fischman. Demsification and Sintering Kinetics in Sintered Silicon Nitride, J. Am. Ceram. Soc. 75 (1992) 1063-1067.

[3] X. Li, X. Yin, L. Zhang, Microstruture and properties fo porous Si_3N_4 ceramics with a dense surface, Int. J. Appl. Ceram. Tec. 8 (2011) 627-636.

[4] K. Okada, K. Fukuyama, Characterization of Surface-Oxidized Phase in Silicon Nitride and Silicon Oxynitride Powders by X-ray Photoelectron Spectroscopy, J. Am. Ceram. Soc. 78 (2010) 2021-2026.

[5] S. Hampshire, M. J. Pomeroy, Grain boundary glasses in silicon nitride: A review of chemistry properties and crystallization, J. Eur. Ceram. Soc. 32 (2012) 1925-1932.

[6] C. Xu, Y. Cai, K. Flodstrum, Z. Li, S. Esmaeilzadeh, G. Zhang, Spark plasma sintering of B_4C ceramics: the effects of milling medium and TiB_2 addition, Int. J. Refract. Met. Hard Mater. 30 (2012) 139-144.

[7] T. Nishimura, M. Mitomo, Fabrication of silicon nitride nano-ceramics by spark Plasma sintering, Mater. Lett. 14 (1995) 1046-1047.

[8] C. H. Lee, H. Lu, Influence of conductive Nano-TiC on Microstuctural Evolution of Si_3N_4-Based Nanocompositcs in Spark Plasma Sintering, J. Am. Ceram. Soc. 94 (2011) 959-967.

[9] L. Diaz, W. Solis, Spark plasma Sintered Si_3N_4 / TiN Nanocompositcs obtained by a colloidal Processing Route, Mater. Lett. 10 (2016) 1-10.

[10] G. Bernard-Granger, C. Guizard, Spark sintering of a commercially available Granulated zirconia powder: Sintering path and hypotheses about the mechanism controlling densification, Acta. Mater. 55 (2007) 3493-3504.

[11] J. P. Poirier, Plasticitéà haute temperature des solides cristallins, Eyrolles, Paris, 1976.

[12] B. M. Moshtaghioun, A L. Ortiz, D. Gomez-Garcfa, A. Domfinguez-Rodriguez, Densification of B_4C nanopowders with nanograin retention by spark-plasma sintering, J. Eur. Ceram. Soc. 35 (2015) 1991-1998.

[13] L. Cheng, S. Jiang, Q. Ma, Z. Shang, S. Liu, Sintering behavior and microwave properties of dense $0.7CaTiO_3$-$0.3NdAlO_3$ ceramics with sub-micron sized grains by spark plasma sintering, Scripta. Mater. 115 (2016) 80-83.

[14] M. Zhang, T. Yuan, R. Li, S. Xie, M. Wang, Q. Weng, Densification mechanisms and microstructural evolution during spark plasma sintering of boron carbide powders, Ceram. Int. 44 (2018) 3571-3579.

[15] S. Deng, T. Yuan, R. Li, F. Zeng, G. Liu, X. Zhou, Spark plasma sintering of pure tungsten powder:densification kinetics and grain growth, Powder. Technol. 310 (2017) 264-271.

[16] C. Greskovich, S. Prochazka, Observations on the α/β-Si3N4 transformation, J. Am. Ceram. Soc. 60 (1977) 341-350.

[17] A. Rosenflanz, I. W. Chen, Kinetics of phase transformations in SiAlON ceramics: Effects of cation size, composition and temperature, J. Eur. Ceram. Soc. 19 (1999) 2325-2335.

[18] R. M. German, P. Suri, Review: Liquid phase sintering, J. Mater. Sci. 44 (2009) 1-39.

[19] M. Kitayama, K. Hirao, Thermal Conductivity of β-Si_3N_4: Effect of Rare-Earth

(RE=La, Nd, Gd, Y, Yb, and Sc) Oxide Additive, J. Euro. Ceram. Int. 84 (2001) 353-358.

[20] D. C. Lam, F. F. Lange, A. G. Evans, Mechanical properties of partically dense alumina produced from powder compacts, J. Am. Ceram. 77 (1994) 2113-2117.

[21] R. J. Brattom, G. R. Terwilliger, S. M. Ho, Densification phenomena in the hotpressing of spinel, J. Mater. Sci. 7 (1972) 1363-1368.

[22] N. Shibata, S. J. Pennycook, Observation of rare-earth segregation in silicon nitride ceramics at subnanometre dimensions, Nature. 428 (2004) 730-733.

[23] E. Y. Sun, P. F. Becher, Microstructure design of silicon nitride with improved Fracture toughness: Effects of Yttria and Alumina additives, J. Am. Ceram. Soc. 81 (1998) 2831-2840.

[24] R. L. Satet, M. J. Hoffmann, Grain growth anisotropy of β-silicon nitride in rare-earth doped oxynitride glasses, J. Eur. Ceram. Soc. 24 (2004) 3437-3445.

[25] H. J. Kleebe, M. Cinibulk, Transmission electron microscopy characterization of a ceria-fluxed silicon nitride, J. Mater. Sci. Lett. 12 (1993) 70-72.

[26] M. Yoshiya, I. Tanaka, Atomic-level modeling and computation of intergranular glassy film in high-purity Si_3N_4 ceramics, J. Eur. Ceram. Soc. 32 (2012) 1301-1311.

[27] V. V. Skorokhod, Processing, microstructure, and mechanical properties of B_4C-TiB_2 particulate sintered composites,Part Ⅰ. Fracture and mechanical properties, Powder Metall. Met. 39 (2000) 504-513.

[28] (a) M. F. Ashby, Scr. Metall. 3 (1969) 837;(b) G. W. Greenwood, Scr. Metall. 4 (1970) 171.

[29] J. G. Santanach, A. Weibel, C. Estournes, Q. Yang, C. Laurent, A. Peigney, Spark plasma sintering of alumina study of parameters, formal sintering analysis and hypotheses on the mechanism involved in densification and grain growth, Acta. Mater.

59 (2015) 1991-1998.

[30] M. Gendre, A. Matre, G. Trolliard, A study of the densification mechanisms during spark plasma sintering of zirconium (oxy-) carbide powders, Acta. Mater. 58 (2010) 2598-2609.

Table and Figures Captions:

Fig.1 The effect of SPS temperature on densification rate

Fig.2Densification curves of Si_3N_4 ceramics sintered by SPS

Fig.3 Crystal structure and phase constituent of Si_3N_4 ceramics prepared under various SPS conditions：(a) 1550-1700 ℃, 30 MPa；(b) 1600 ℃, 30 -50 MPa

Fig.4 Fracture morphology of Si_3N_4 ceramics under different discharge plasma sintering conditions:(a) 1550 ℃, 30 MPa；(b) 1550 ℃, 40 MPa；(c) 1550 ℃, 50 MPa；(d) 1600 ℃, 30 MPa；(e) 1600 ℃, 40 MPa；(f) 1600 ℃, 50 MPa；(g) 1650 ℃, 30 MPa；(h) 1700 ℃, 30 MPa.

Fig.5 Grains average size of Si_3N_4 ceramics by SPS.

Fig.6 Sintering sress exponentes of Si_3N_4 ceramics SPSed under various conditions

Fig.7 Microstructure of Si_3N_4 ceramics SPSed at 1600℃ with 30 MPa (a) TEM bright field image，(b) Elements mapping of particle，(c) HR-TEM of particle

Tab.1 The mechanical properties of SPSed Si_3N_4 samples

Figures

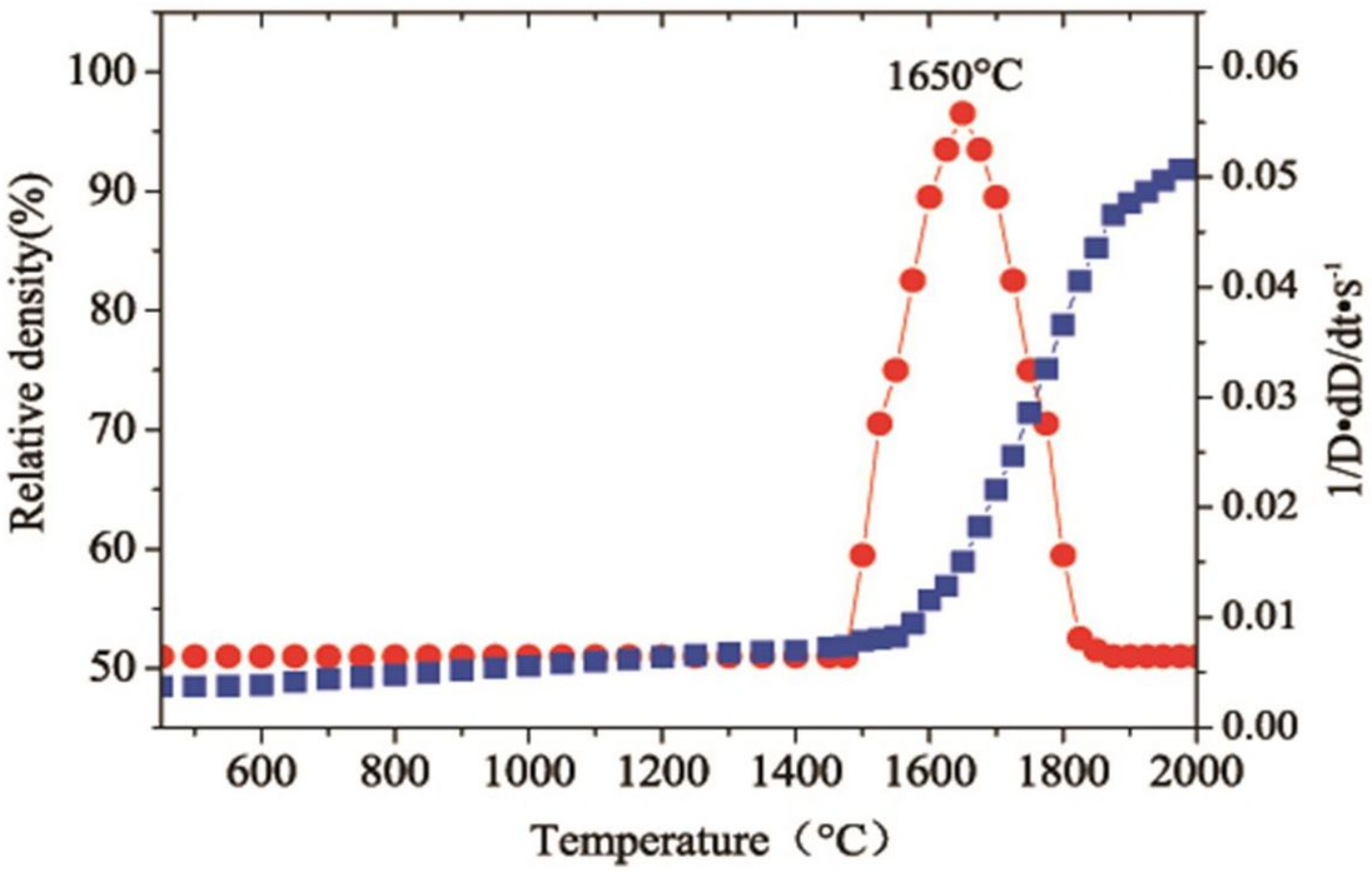

Figure 1

Liu et al. The effect of SPS temperature on densification rate

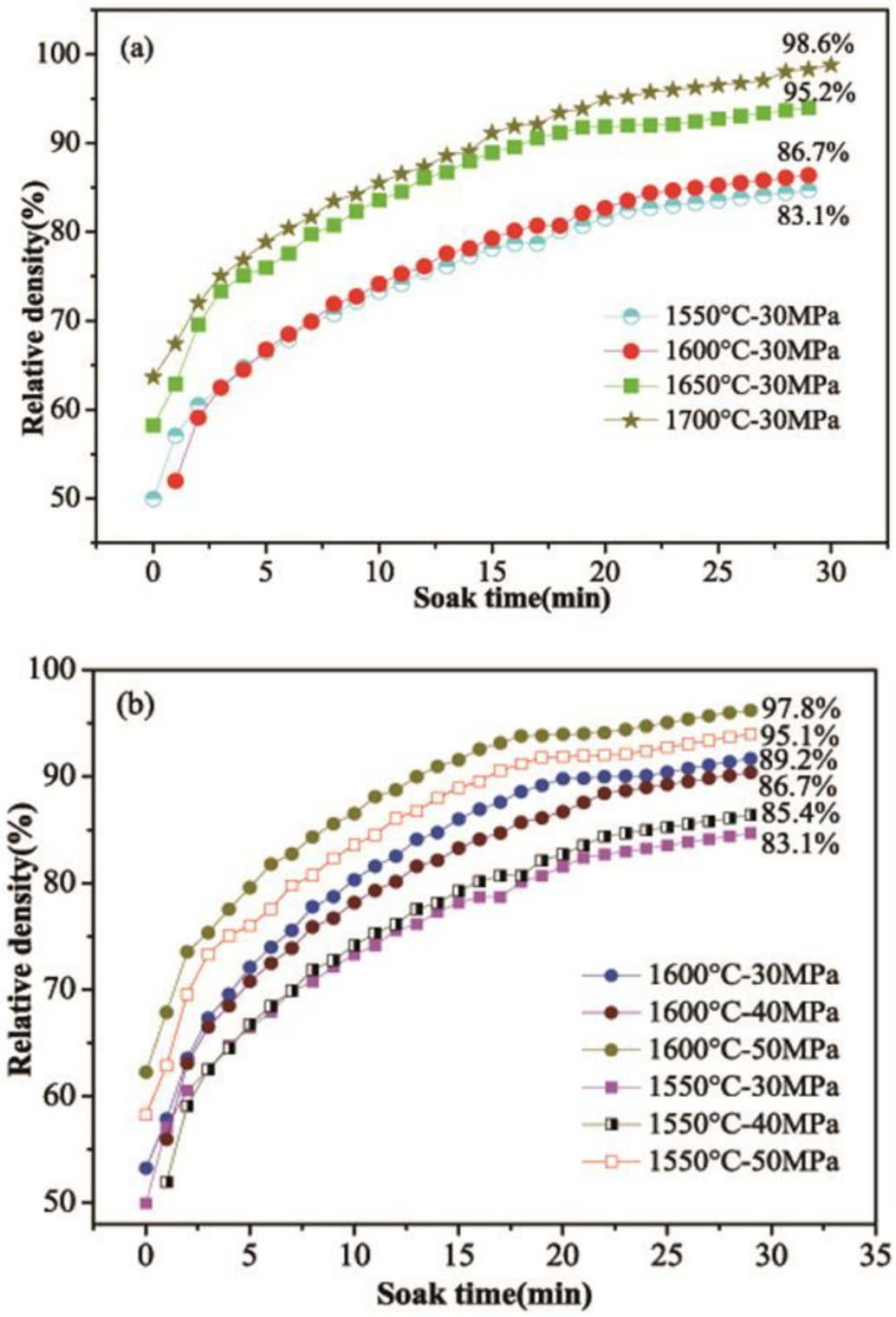

Figure 2

Liu et al. Densification curves of Si3N4 ceramics sintered by SPS

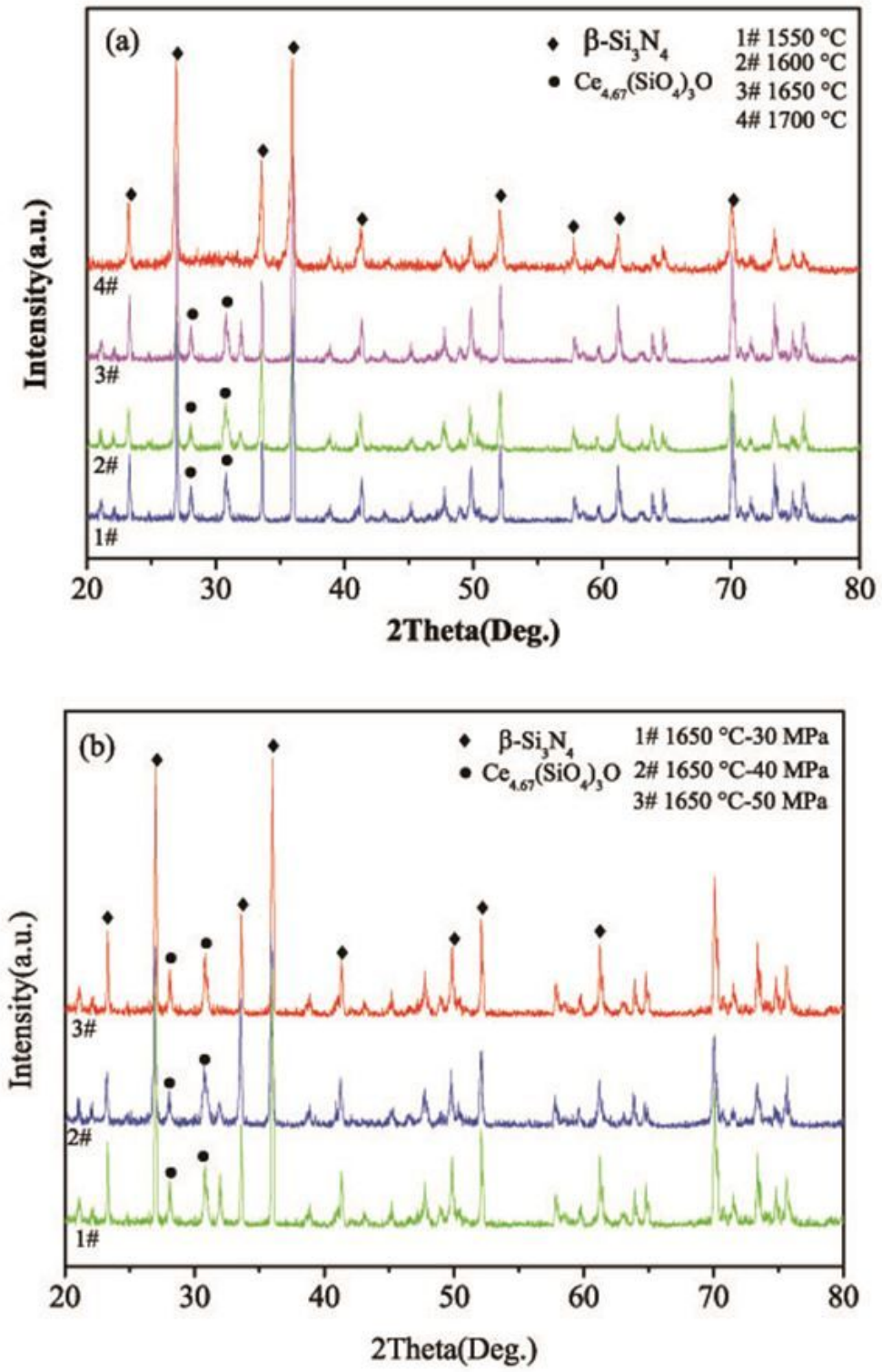

Figure 3

Liu et al. Crystal structure and phase constituent of Si3N4 ceramics prepared under various SPS conditions：(a) 1550-1700 ℃, 30 MPa；(b) 1600 ℃, 30 -50 MPa

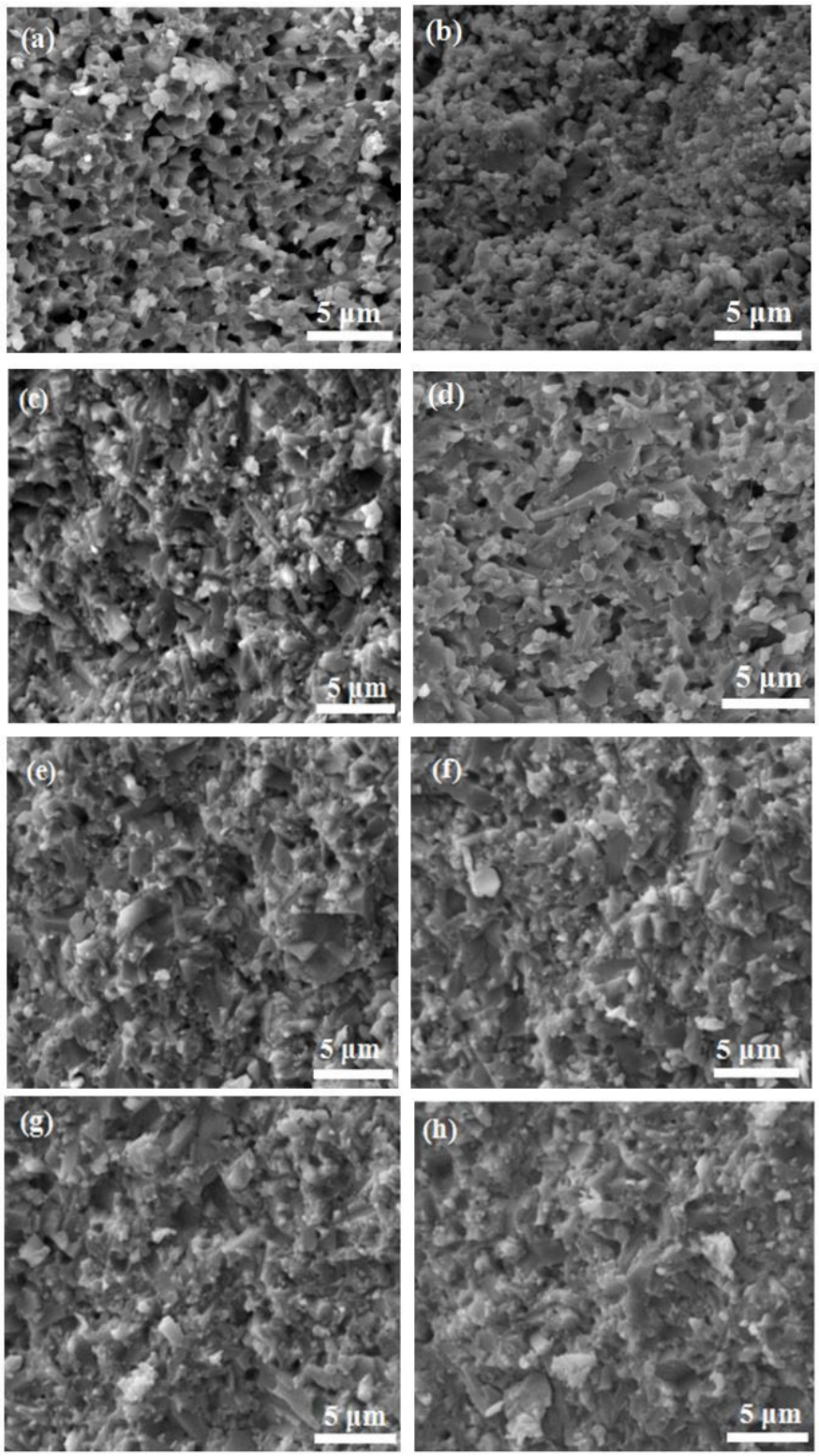

Figure 4

Liu et al. Fracture morphology of Si3N4 ceramics under different discharge plasma sintering conditions: (a) 1550 ℃, 30 MPa；(b) 1550 ℃, 40 MPa；(c) 1550 ℃, 50 MPa；(d) 1600 ℃, 30 MPa；(e) 1600 ℃, 40 MPa；(f) 1600 ℃, 50 MPa；(g) 1650 ℃, 30 MPa；(h) 1700 ℃, 30 MPa.

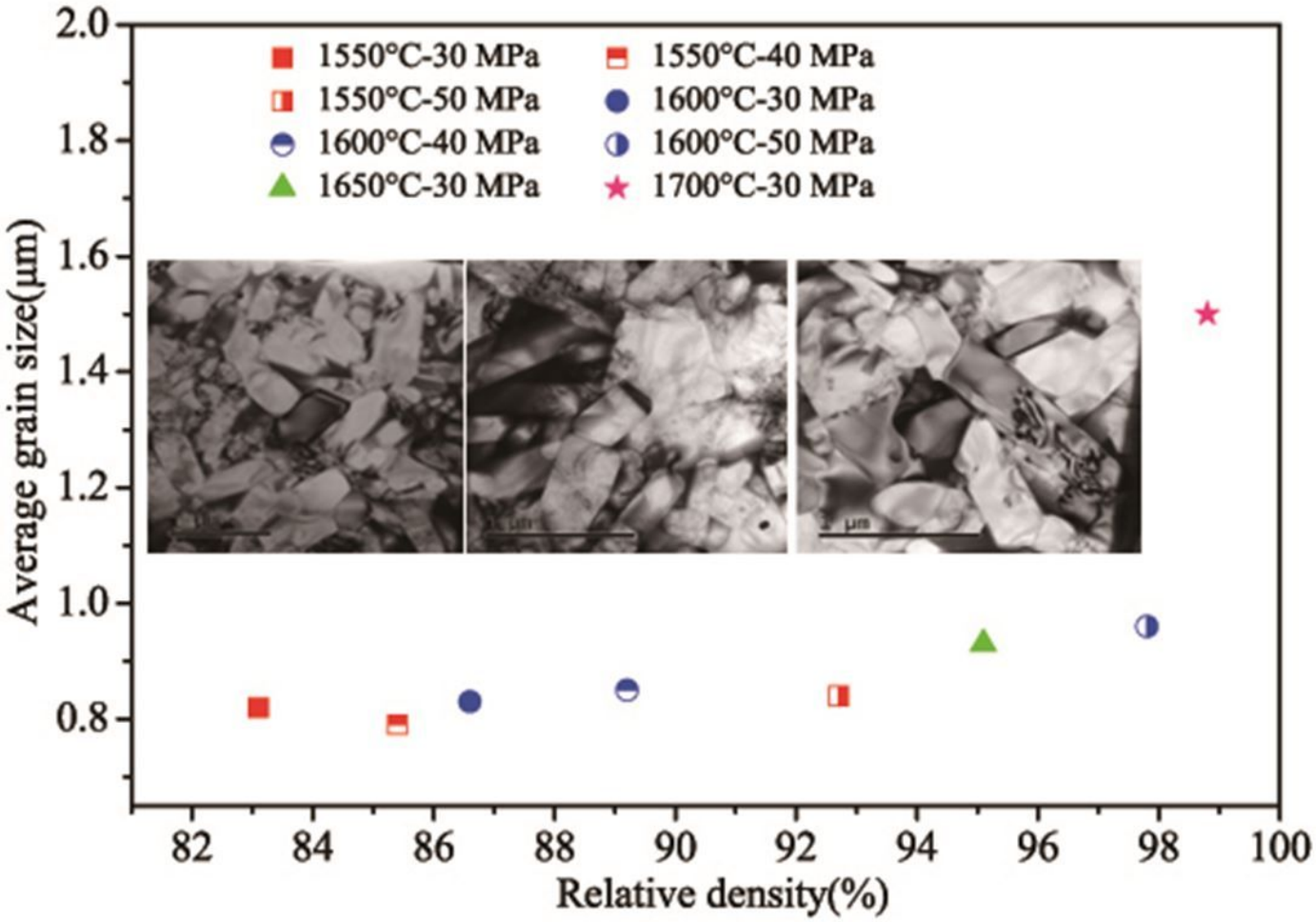

Figure 5

Liu et al.Grains average size of Si3N4 ceramics by SPS

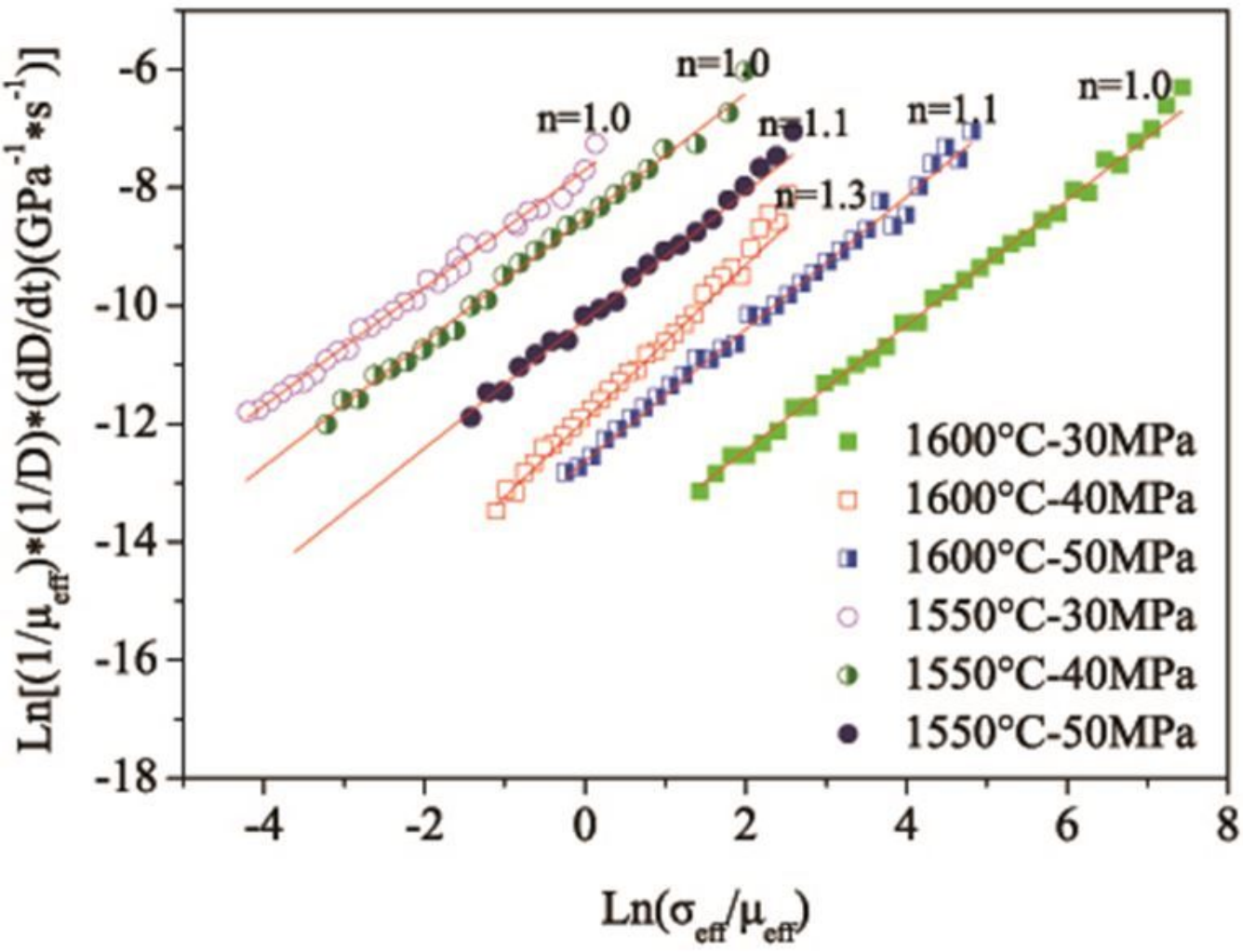

Figure 6

Liu et al. Sintering sress indexes of Si3N4 ceramics SPSed under various conditions

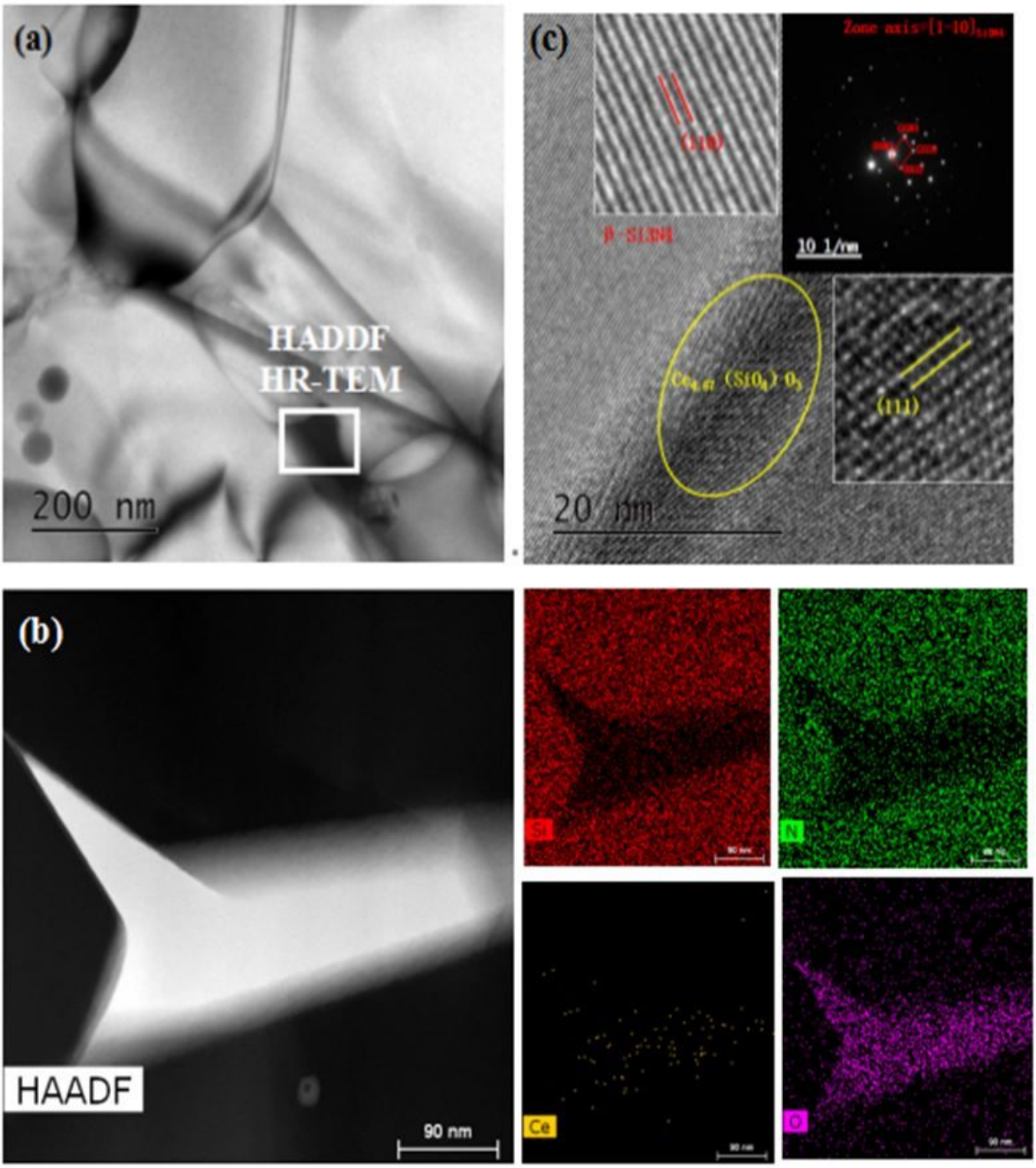

Figure 7

Liu et al. Microstructure of Si3N4 ceramics SPSed at 1600℃ with 30 MPa (a) TEM bright field image, (b) Elements mapping of particle, (c) HR-TEM of particle